nature structural & molecular biology

Structure of the cholera toxin secretion channel in its closed state

Steve L Reichow[1,3], Konstantin V Korotkov[1,3], Wim G J Hol[1] & Tamir Gonen[1,2]

The type II secretion system (T2SS) is a macromolecular complex spanning the inner and outer membranes of Gram-negative bacteria. Remarkably, the T2SS secretes folded proteins, including multimeric assemblies such as cholera toxin and heat-labile enterotoxin from *Vibrio cholerae* and enterotoxigenic *Escherichia coli,* respectively. The major outer membrane T2SS protein is the 'secretin' GspD. Cryo-EM reconstruction of the *V. cholerae* secretin at 19-Å resolution reveals a dodecameric structure reminiscent of a barrel, with a large channel at its center that contains a closed periplasmic gate. The GspD periplasmic domain forms a vestibule with a conserved constriction, and it binds to a pentameric exoprotein and to the trimeric tip of the T2SS pseudopilus. By combining our results with structures of the cholera toxin and T2SS pseudopilus tip, we provide a structural basis for a possible secretion mechanism of the T2SS.

One or more variants of the T2SS occur in many proteobacteria, including several important pathogens of humans and plants[1]. One such pathogenic bacterium is *V. cholera*, which uses its T2SS to secrete, among other proteins, the major virulence factor cholera toxin in a folded state from the periplasm across the outer membrane[2,3]. Heat-labile enterotoxin, produced by enterotoxigenic *E. coli* (ETEC), is related to cholera toxin in sequence and structure and is also secreted by a T2SS[4,5]. Both cholera toxin and heat-labile enterotoxin are heterohexamers composed of one A and five B subunits (AB_5). Although the secretion signals of proteins secreted by the T2SS are still unknown, in the case of both cholera toxin and heat-labile enterotoxin, the secretion signal resides in the B pentamer and not in the A subunit[6,7]. Owing to the apparent lack of a linear secretion signal sequence, it has been suggested that the secretion signal is instead a structural motif present in the native or near-native protein structure[8–11].

The T2SS is a multiprotein macromolecular machine that spans both the inner and outer membrane of the bacteria[12,13]. On its cytosolic side, the T2SS contains a secretion ATPase called GspE, which is associated with an inner-membrane platform comprising multiple copies of the proteins GspL, GspM, GspF and GspC. A second T2SS subassembly is the so-called pseudopilus, which consists of the pseudopilins GspG, GspH, GspI, GspJ and GspK. The pseudopilus is thought to act as a plug and/or piston during the secretion of proteins and of toxins[14–16].

The major outer-membrane protein of the T2SS is the secretin GspD, which forms one of the largest multimeric assemblies in the outer membrane of bacteria. In *Pseudomonas* species, GspD is also called XcpQ; in *Vibrio* species, it is called EpsD. The secretins form a diverse family of proteins, occurring in a wide variety of bacteria, with a complex and variable multidomain structure. Homologs of the T2SS-related secretins are crucially important components of other macromolecular assemblies such as the type III secretion system (T3SS), the type IV pilus biogenesis system (T4PBS) and the filamentous phage assembly system[17–26]. These systems occur in a range of bacteria and perform many sophisticated functions, including bacteriophage extrusion, pilus extension and retraction, twitching motility, DNA uptake, injection of proteins directly into target cells and secretion of proteins into the extracellular milieu.

Here we used electron cryo-EM and single-particle reconstruction to determine the 19-Å-resolution structure of the T2SS secretin GspD from *V. cholerae* (*Vc*GspD). Previous secretin reconstructions determined by cryo-EM have been reported with comparable resolutions[21,23]; however, the *Vc*GspD reconstruction reported here is, structurally, the most complete representation of a T2SS secretin to date. The *V. cholerae* secretin appears as a dodecameric channel of 200 Å in length, with a largely unobstructed periplasmic vestibule. This vestibule contains a constriction site and is separated by a gate from an extracellular chamber that is connected to the extracellular milieu by a cap. Crystal structures of periplasmic GspD subdomains fit well within the contoured features of the cryo-EM map. This conserved periplasmic domain is shown to bind to a T2SS exoprotein and also to the pseudopilus tip complex. By combining our results with structural data on a large exoprotein, the ~85-kDa cholera toxin, and our recent crystal structure of the tip of the pseudopilus of the T2SS, we provide a structural basis for a possible secretion mechanism of exoproteins by the T2SS in which the secretin constriction site has a crucial role.

[1]Department of Biochemistry, University of Washington, Seattle, Washington, USA. [2]Howard Hughes Medical Institute, University of Washington, Seattle, Washington, USA. [3]These authors contributed equally to this work. Correspondence should be addressed to T.G. (tgonen@u.washington.edu) or W.G.J.H. (wghol@u.washington.edu).

Received 15 February; accepted 27 July; published online 19 September 2010; doi:10.1038/nsmb.1910

RESULTS

Cryo-EM of recombinant *V. cholerae* GspD

We carried out overexpression of the full-length *Vc*GspD in *E. coli*, isolated the intact channels from the membrane fraction and purified them to homogeneity (**Fig. 1a**,**b**). Initially, we assessed the suitability of the preparation for analysis under cryogenic conditions using negative-stain EM (data not shown). We prepared purified *Vc*GspD for cryo-EM using a vitrification robot (Vitrobot, FEI) and continuous carbon copper grids, rather than holey carbon grids, to circumvent particle orientation difficulties in ice (**Fig. 1c**). We then selected ~20,000 vitrified *Vc*GspD particles in Ximdisp[27] from electron micrographs and classified them using reference-free computational alignment routines in SPIDER[28] (**Fig. 1c**, inset).

In side views, the *Vc*GspD particles appear as striated, elongated structures (indicated by arrowheads in **Figure 1c** and the lower inset panel). A strong band of density bisects the center of the *Vc*GspD particle and seems to separate the periplasmic and the extracellular domains of the channel. When viewed axially along the channel pore axis, the *Vc*GspD appears as a ring of density with weak radial densities, or 'spokes' (**Fig. 1c**, upper inset panel). We used these radial spokes to assign the rotational symmetry to *Vc*GspD channels using real-space symmetry averaging and rotational power spectra analysis[29] (**Supplementary Fig. 1**). This analysis strongly suggests that *Vc*GspD is a dodecamer and is in agreement with mass estimates obtained by size-exclusion chromatography (**Fig. 1a**).

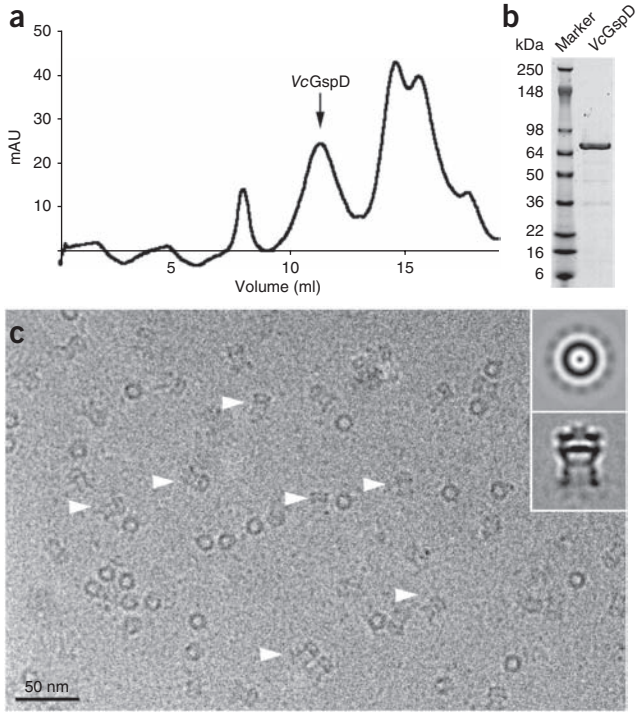

Figure 1 Purification and cryo-EM of the cholera toxin secretion channel *Vc*GspD. (**a**) *Vc*GspD channels were purified to homogeneity by size-exclusion chromatography. The intact channels eluted as an ~0.9-MDa species (arrow). (**b**) Coomassie blue–stained SDS-PAGE of purified *Vc*GspD (~74 kDa). (**c**) Electron micrograph of vitrified *Vc*GspD channels. Inset, above, representative class averages of *Vc*GspD particles. In top views, looking down the channel axis, the particles appear as a ring with a punctate density located at the center of the channel, and weaker densities—spokes—surround the channel. Inset, below, side views (indicated by arrowheads) appear as long, striated channels with a strong central density or 'plug' that bisects the center of the channel.

We carried out the three-dimensional reconstruction of *Vc*GspD in FREALIGN[30] using the best ~10,000 particles with an applied 12-fold rotational symmetry. The resulting density is ~19 Å in resolution, as determined by the 0.5 Fourier shell correlation (FSC) criterion (**Supplementary Fig. 2**). Two-dimensional back-projections of the *Vc*GspD cryo-EM map demonstrated a good fit to the raw image data (data not shown). The density map was contoured at 3.4σ above noise, yielding a ~0.9-MDa molecular mass that is consistent with 12 subunits of *Vc*GspD per particle.

Architecture of the *Vc*GspD secretin channel

The *Vc*GspD cryo-EM density reveals a cylindrical channel assembly of ~155 Å in diameter and ~200 Å in length, with a girdled waist (**Fig. 2**). In side view, the periplasmic domain of the channel is at the bottom followed by an outer-membrane domain in the middle and an extracellular domain at the very top. The surface of the outer-membrane domain seems to be smooth (possibly owing to detergent and/or lipid molecules surrounding the transmembrane domain of the channel), whereas the surface of the periplasmic domain seems to be highly contoured and segmented, with clear 12-fold symmetric features. The 12-fold radial spoke densities observed in projection averages are found radiating off the bottom of the periplasmic domain when the map is displayed at a slightly lower contour level (compare **Figure 1c**, inset, with **Figure 2b** and **Supplementary Fig. 1**). These spoke features may correspond to the disordered N-terminal signaling sequence that is retained by *Vc*GspD in our *E. coli* expression system (see Online Methods). Projection views of the *Vc*GspD reconstruction reveal additional 12-fold symmetric features that can be observed throughout the architecture of the channel (**Supplementary Fig. 1**).

Additional features become apparent in a cross-section through the *Vc*GspD channel (**Fig. 2c**). The periplasmic domain of the channel accounts for ~125 Å of the total 200 Å length of the channel. The opening to the periplasmic vestibule is ~75 Å in diameter, and its walls are ~40 Å thick. Approximately two-thirds of the way into the periplasmic vestibule, we identify a constriction that narrows the channel's internal diameter to ~55 Å. A continuous density, which we refer to as the periplasmic gate, seals off the periplasmic vestibule from the extracellular chamber of the channel.

The outer membrane and the extracellular domains of *Vc*GspD account for 75 Å of the total 200-Å length of the channel. Immediately following the periplasmic gate, the extracellular domain of *Vc*GspD appears as a chamber ~100 Å in diameter (**Fig. 2c**). A puckered density that forms a second gate structure caps the top of this chamber. We refer to this second gate as the extracellular gate. In sharp contrast with the periplasmic gate, which appears as a solid density, the extracellular gate seems to leave a small opening of ~10 Å in diameter, suggesting that this gate does not form a tight seal across the channel pore. The walls surrounding the extracellular chamber are ~20 Å thick and seem to be smooth, possibly owing to the presence of detergent and/or lipid molecules as discussed above, but also consistent with the predicted β-barrel topology for this domain of *Vc*GspD and related secretins[18].

Global aspects of our *Vc*GspD architecture agree with the cryo-EM reconstruction[23] of the T2SS secretin from *Klebsiella oxytoca* (*Ko*GspD), also called PulD. The nontrypsinized *Ko*GspD multimer is also a 12-fold symmetric channel, with outer and inner diameters as observed in the *Vc*GspD structure. However, the membrane-spanning segment of *Ko*GspD was relatively poorly defined and the periplasmic vestibule of *Vc*GspD is ~80 Å longer than that measured in the *Ko*GspD study (**Supplementary Fig. 3**). This

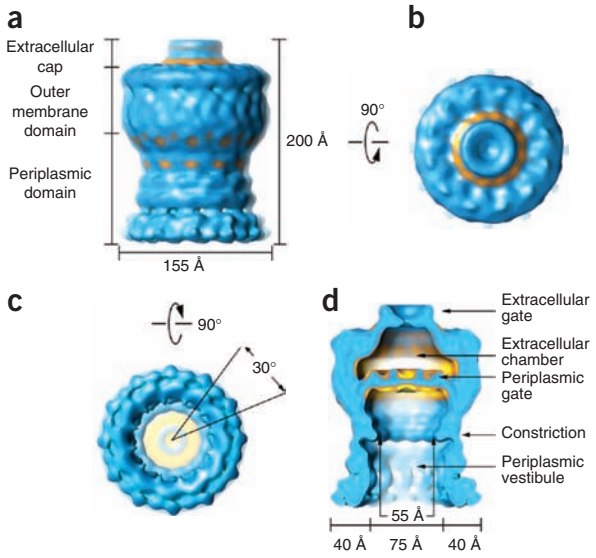

Figure 2 Three-dimensional electron cryo-EM reconstruction of *Vc*GspD. (**a**–**c**) Side (**a**), top (**b**) and bottom (**c**) views of the dodecameric *Vc*GspD reconstruction at 19-Å resolution. In side view, three domains are identified from bottom to top as the periplasmic domain, the outer-membrane domain and the extracellular cap. (**d**) A slice view through the channel reveals the periplasmic vestibule, a constriction, the periplasmic gate, an extracellular chamber and an extracellular gate. The extracellular chamber is ~100 Å wide, whereas the periplasmic vestibule is ~75 Å in diameter. The periplasmic constriction narrows the vestibule to ~55 Å.

additional density has allowed us to place the recently determined crystal structures of the N-terminal subdomains of *Ec*GspD[31] into the *Vc*GspD EM reconstruction, as discussed below. The entrance to the periplasmic vestibule in the *Ko*GspD reconstruction was ~55 Å wide, which we can now attribute to the constriction site in our more complete reconstruction. The extracellular gate in our *Vc*GspD reconstruction is a feature that has not been previously observed in reported secretin reconstructions. We propose that this domain has a crucial role in the secretion mechanism of the T2SS as the final channel gate that allows exoprotein release into the extracellular environment (see Discussion).

The secretin architecture in diverse secretion systems

Members of the bacterial outer-membrane secretin family are found in the T2SS, the T3SS, the T4PBS and the filamentous phage secretion systems[17,18]. We analyzed the amino acid sequences of secretins from these four secretion systems and compared their domain organization (**Fig. 3a** and **Supplementary Fig. 4**). All members of the secretin family contain a defining large C-terminal core domain, called the secretin domain (Pfam family PF00263 (ref. 32); cyan in **Fig. 3a** and **Supplementary Fig. 4**). Variable regions that are secretion system and species-specific flank this defining core domain. The N-terminal region of members of the secretin family is modular, and all of these secretins contain, at a minimum, (i) the N-terminal N0-like and (ii) the N3-like subdomains directly preceding the C-terminal defining secretin domain (**Fig. 3a**). These sequence-based analyses indicate both a considerable similarity and substantial differences in the domain organization of secretins in the outer membrane of many bacterial secretion and biogenesis systems.

The domain architecture of secretins from the T2SS and T3SS seem to be most similar among these four systems, both containing N-terminal modules named the N0, N1 and N3 subdomains (**Fig. 3a** and **Supplementary Fig. 4**). The N0 subdomains of the T2SS and T3SS assume the same topology despite low amino acid sequence identity, with a fold related to the signaling domain of TonB-dependent receptors and bacteriophage tail proteins[31,33]. The structures of the T2SS N1 and N2 subdomains have the same KH domain fold, and it has been predicted that the T2SS N3 subdomain has the same structure, which is also shared with the T3SS N1 and N3 subdomains (**Supplementary Figs. 4** and **5**). Notably, T3SS secretins lack the N2 subdomain that is found in the T2SS secretins.

Secretins from the T3SS have been studied by single-particle EM as part of the assembled T3SS complex, in both its closed and open states[24–26] (**Fig. 3b**). Like the T2SS, the T3SS is a large multiprotein complex that spans both the inner and outer membrane of bacteria. The T3SS base complex mainly consists of the outer-membrane secretin, sitting on top of a T3SS inner-membrane complex (**Fig. 3b**, middle). The cryo-EM reconstruction of the T2SS *Vc*GspD secretin resembles that of the T3SS secretin in the closed state without needle (**Fig. 3b**, compare the left panel with the middle panel). In both structures the large periplasmic gate appears closed and the ~55-Å-wide periplasmic constriction is apparent, approximately equally distant from the periplasmic gate. The reconstructions of the fully assembled T3SS[24,26] noticeably lack the extracellular gate observed in the *Vc*GspD secretin. This feature may therefore be specific to the T2SS secretins; however, it is also possible that this domain was not resolved in the available T3SS reconstructions. Further structural studies will be required to dissect these structural differences.

The outer-membrane pore-forming channel from the type IVa secretion system (T4aSS) has been recently characterized by X-ray crystallography[34] and as part of the assembled T4aSS by cryo-EM[35]. The T4aSS outer-membrane channels do not seem to be genetically related to the secretin family of outer-membrane channels[34]. Indeed, overall they seem to be structurally unique, and also different from the type IVb secretion system[36–38]. Still, a side-by-side structural comparison does reveal some common global structural outside shape features, although the internal shape is distinctly different (compare for example, **Figure 3b** with Figure 4c from ref. 34; **Supplementary Fig. 6**).

Molecular modeling of GspD N0–N3 and substrate interaction

The periplasmic domain of *Vc*GspD density is modular. In cross-section, the walls of this domain that form the periplasmic vestibule of the channel appear as concentric rings of density (**Fig. 2c**). Indeed, the periplasmic N terminus of secretins from the T2SS contains four periplasmic subdomains, N0–N3 (**Figs. 3a** and **4**). We recently published the crystal structure of the N-terminal periplasmic subdomains N0-N1-N2 from the homologous ETEC GspD secretin[31]. The crystal structure revealed a modular architecture, composed of three consecutively linked domains with mixed α/β topology. The modular features resolved within the periplasmic domain of the *Vc*GspD cryo-EM map correspond well with the modular architecture observed in the crystal structures of periplasmic *Ec*GspD. Although our crystal structure did not include N3, this domain is related in sequence to both N1 and N2 with strong predicted structural homology[31] (Pfam family PF03958; ref. 32).

As the sequence similarity between *Ec*GspD and *Vc*GspD is very high, with 54% amino acid sequence identity for these subdomains (**Supplementary Fig. 4**), we used the crystal structure of periplasmic *Ec*GspD to fit the N0-N1-N2-N3 subdomains. We first used the program SymmDock[39] to generate 12-fold-symmetrical rings (**Fig. 4a**). The N0 and N1 domains were treated as a single complex, as observed

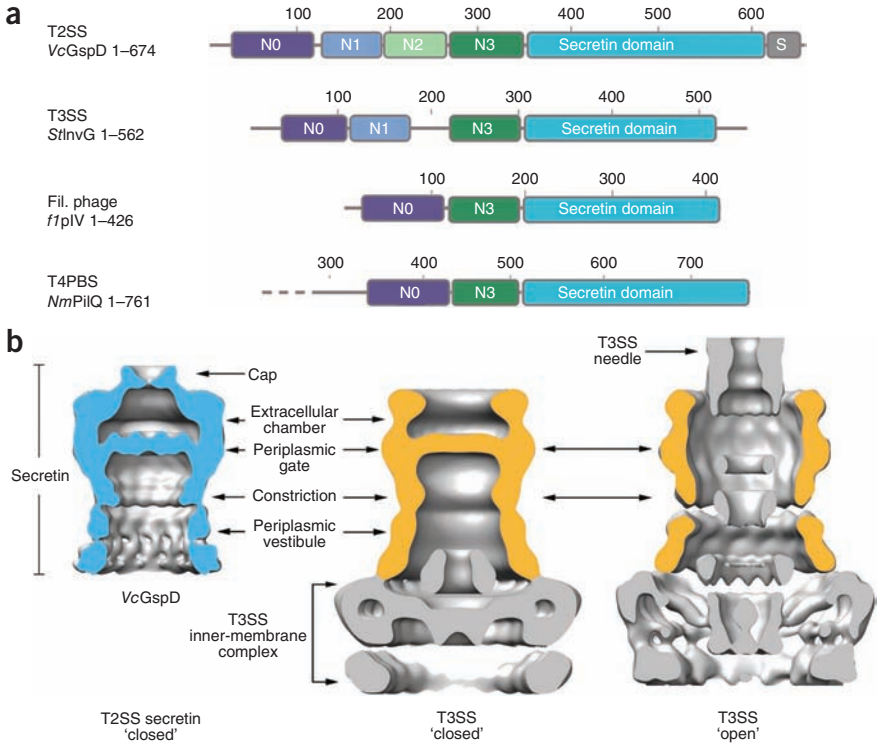

Figure 3 The secretin architecture is conserved in different secretion systems. (**a**) Domain architecture of secretins from the T2SS, the T3SS, the filamentous phage assembly system and the T4PBS. Members of the secretin superfamily contain a C-terminal secretin core homology domain[17,18] (cyan). The T2SS secretins generally contain four periplasmic subdomains, termed N0–N3. The N0 subdomain (dark blue) is located at the N terminus and is followed by the three structurally homologous subdomains, N1–N3 (blue, green and dark green, respectively). A T2SS-specific domain, termed the S-domain (gray), is located at the very C terminus. Secretins from other systems share a similar architecture, composed of the secretin domain and at least two periplasmic subdomains that are structurally equivalent to N0 and N3 of *Vc*GspD. (**b**) Structural comparison of the *Vc*GspD density (blue, left) to single-particle reconstructions of the T3SS in its closed state (middle) (EMDB 1224)[26] and to the fully assembled T3SS needle complex in its open state (right) (EMDB 1617)[24]. The outer-membrane T3SS secretin sits on top of a large inner-membrane complex (gold, middle and right). *Vc*GspD seems to be in its closed state (compare left panel with middle panel).

in the crystal structure of periplasmic *Ec*GspD, whereas the N2 and N3 ring models were treated independently because these are tethered by flexible linkers (**Supplementary Fig. 4**).

The fitted periplasmic ring models match well within the modular contours of the *Vc*GspD cryo-EM map (**Fig. 4** and **Supplementary Fig. 7**). The N0-N1 ring fitted into the ~40 Å lobe of density at the very bottom of the *Vc*GspD periplasmic vestibule. The N2 and N3 rings fitted well directly above the N0-N1 ring (**Fig. 4a**). This arrangement matched the contours of the periplasmic domain, placing the N2 subdomain into the central segment of this region and positioning the N3 subdomain snuggly into the volume encompassing the periplasmic constriction. The fit of the N3 subdomain at the periplasmic constriction is consistent with proteolysis studies of *Ko*GspD[23] (**Supplementary Fig. 3**).

To investigate the possible functional role of the GspD periplasmic domain, we characterized by surface plasmon resonance (SPR) the interactions between (i) the periplasmic domain of the secretin from enterotoxigenic *E. coli* (specifically the fragment containing *Ec*GspD subdomains N0-N1-N2 (ref. 31)), (ii) the B-pentamer of heat-labile enterotoxin (LT-B_5), which is secreted by the T2SS of enterotoxigenic *E. coli*[5] and (iii) the trimeric complex *Ec*GspK–GspI–GspJ[40], which forms the tip of the T2SS pseudopilus (**Fig. 4b**). Our analysis showed that the secretin *Ec*GspD binds independently to the exoprotein heat-labile enterotoxin and to the pseudopilus tip complex. However, we did not detect binding between heat-labile enterotoxin and the pseudopilus tip complex (data not shown), which may reflect either a lack of interaction or a requirement for additional T2SS proteins. Together, these data suggest that the secretin periplasmic domain has an important functional role in recognition of both the exoprotein and the secretion machinery.

The N3 periplasmic domain fits into the constriction of the *Vc*GspD density (**Fig. 4a**). The N3 periplasmic domain seems to be highly conserved at the amino acid level, even in distantly related secretins (**Fig. 3a** and **Supplementary Fig. 4**), suggesting that this domain has a conserved mechanistic role in these secretion systems. The evidence for such a role is supported by a recent study that identified several amino acids within the N3 domain of the secretin pIV from the filamentous phage assembly system that, when mutated, resulted in a 'leaky' channel phenotype[41]. To gain further insight into the mechanistic role of this conserved domain, we placed the structure of the cholera toxin heterohexamer AB_5 (ref. 42) into the *Vc*GspD secretin density (**Fig. 4c**). Our analysis shows that the periplasmic vestibule of the secretin channel is large enough to accommodate the cholera toxin, although it is a snug fit. The ~65-Å-wide cholera toxin structure fits well within the ~75-Å-wide vestibule created by the N0–N2 domains, without any obvious steric hindrance. In sharp contrast, the cholera toxin cannot fit through the constriction formed by N3 (~55 Å in diameter) without a major conformational change in the secretin. The N3 subdomain may therefore be important for T2SS exoprotein recognition and secretion, at least for larger exoproteins such as the ~85-kDa cholera toxin and heat-labile enterotoxin. For smaller exoproteins, for example, the ~36-kDa pectate lyase from *Dickeya dadantii* (*Erwinia chrysanthemi*)[43], a different process may operate, as such small proteins would not be blocked by the T2SS constriction. It is noteworthy that the diameter of the GspK–GspI–GspJ tip of the pseudopilus is ~54 Å (ref. 40), that is, essentially the same as the cross-section of the *Vc*GspD constriction. Therefore, in such cases the tip of the pseudopilus might interact with the constriction and cause conformational changes that lead to opening of the gate in the T2SS secretin channel.

DISCUSSION

The mechanism of protein secretion by the T2SS is essentially unknown. The T2SS contains a pseudopilus, which has been suggested to act either as a plug to close the outer-membrane pore or as a piston involved in pushing toxins and other secreted proteins through the secretin pore[14–16]. Our cryo-EM reconstruction of the secretin *Vc*GspD clearly identifies a periplasmic gate, and the channel seems to be in its closed state (**Figs. 2–4**). As the channel is already closed, it seems likely that the function of the pseudopilus in secretion would be

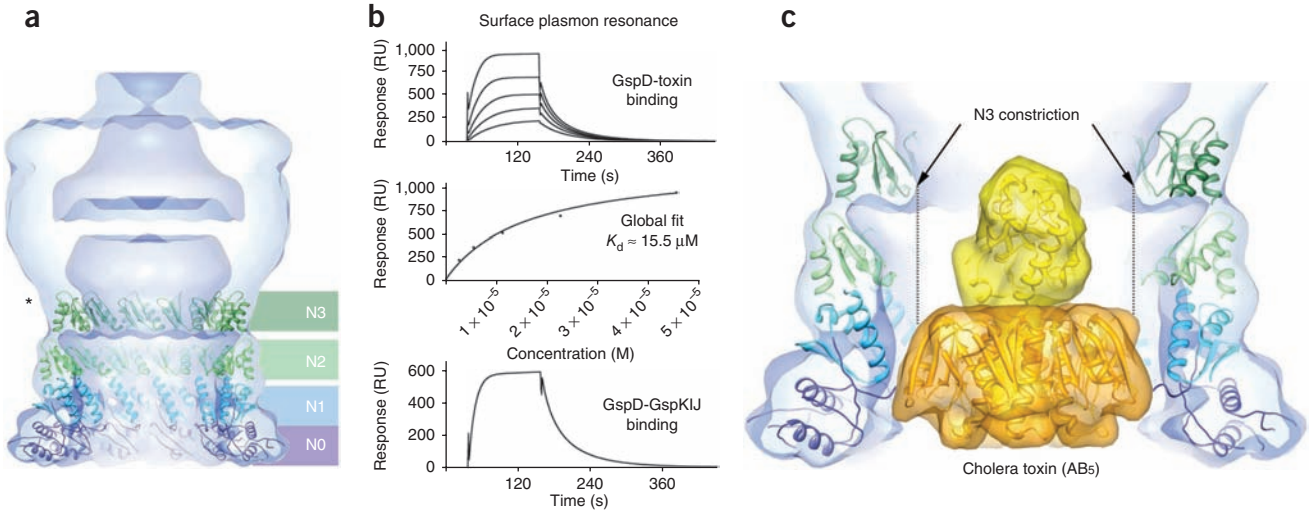

Figure 4 The periplasmic GspD domain contains a conserved N3 constriction and binds to the T2SS exoprotein and pseudopilus tip complex. (**a**) Fitting of 12-member ring models of the *Vc*GspD N-terminal periplasmic domains (N0–N3) into the *Vc*GspD density map. The N0 domain (dark blue) and N1 domain (light blue) are anchored at the bottom of the *Vc*GspD density map. This places the N2 domain (light green) into the central periplasmic domain density and the N3 domain (dark green) into the periplasmic constriction. This placement correlates well with protease cleavage experiments that cut at N3 (asterisk)[23,33]. (**b**) Surface plasmon resonance studies of GspD interaction with an exoprotein and the pseudopilus tip. Above, sensorgram showing binding of the B-pentamer of heat-labile enterotoxin (B_5) to immobilized periplasmic *Ec*GspD. Relative units (RU, vertical) are plotted as a function of time (in seconds, horizontal). Middle, global fit of the equilibrium measurements (RU) shown above versus B_5 concentrations (M) gives a dissociation constant (K_d) of ~15.5 μM. Below, sensorgram showing the binding of the pseudopilus tip complex *Ec*GspK–GspI–GspJ to immobilized periplasmic *Ec*GspD. (**c**) Fitting of the cholera toxin AB_5 heterohexamer (PDB 1S5E)[42] (A subunit, yellow; B subunits, gold) into the *Vc*GspD periplasmic vestibule. The ~65-Å-wide cholera toxin molecule fits well within the ~75-Å vestibule formed by the N0–N2 domains but would not fit through the ~55-Å-wide constriction composed of the N3 domain.

to act as a piston to push exoproteins out; however, it may also serve as a plug to seal the pore once the periplasmic channel gate is opened.

The crystal structures of all pseudopilins have been recently determined, including the ternary complex of GspK–GspI–GspJ at the very tip of the pseudopilus[40,44–47]. In the following paragraphs, we combine this wealth of recent structural information with our new cryo-EM structure of the secretin to show how the piston mechanism for toxin secretion by the T2SS could work, with the secretin constriction having a key role (**Fig. 5**).

The piston secretion model could start with the tip of the pseudopilus interacting with cholera toxin and aligning its helix axis with the pore axis of the secretin. It is also possible that the toxin, and

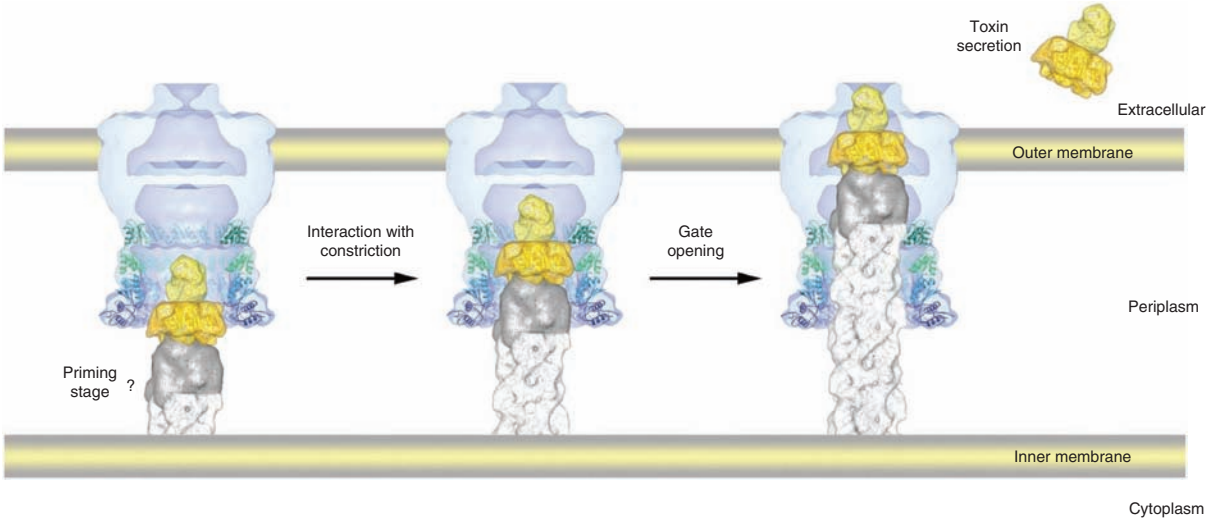

Figure 5 Piston-driven mechanism for protein secretion. The key structural steps that are proposed to occur during protein secretion across the outer membrane by the type 2 secretion system. Left, the T2SS secretin (blue) is in its closed state. Large exoproteins, such as the cholera toxin AB_5 heterohexamer (gold), are proposed to interact with the pseudopilus tip complex (gray) positioned at the inner membrane beneath the secretin channel, or bind directly to the secretin. Middle, the pseudopilus would then extend, acting in a similar way to a piston to push the toxin into the periplasmic vestibule of the secretin and onto the constriction. Right, the interaction between the N3 domain (constriction) and large exoproteins such as the toxin could act as the trigger to open the periplasmic gate, allowing exoproteins to enter the extracellular chamber of the secretin. The final step would involve opening of the extracellular gate, allowing exoproteins to be secreted (see also Discussion).

other exoproteins in general, may first be recruited into the secretin periplasmic vestibule, followed by a second step in which the growing pseudopilus translocates the exoprotein through the secretion machinery[14] (**Fig. 5**, left). Our binding data (**Fig. 4b**) indicate that exoproteins are recruited directly by the secretin by binding to the periplasmic domain of the channel (**Fig. 5**, left). At this stage, the secretin itself is in its closed state. Next, the pseudopilus begins to polymerize and extend, pushing the toxin into the periplasmic vestibule of the secretin (**Fig. 5**, middle). The periplasmic vestibule of the secretin is wide enough to accommodate the toxin and the pseudopilus.

Once the toxin or the tip of the pseudopilus reaches the N3 domain of the secretin (the constriction), the channel will need to undergo a conformational change to open the pore and allow the toxin to be secreted (**Fig. 5**, right). This conformational change may resemble that observed in the T3SS upon needle attachment (**Fig. 3b**, compare the middle panel with the right panel; see also ref. 26). Namely, the secretin N3 constriction would move outward, expanding the constriction from ~55 Å to a larger diameter of ~70–90 Å to let the toxin and pseudopilus pass. At the same time, the periplasmic gate would open and the toxin could then enter the extracellular chamber of the secretin (**Fig. 5**, right).

No pseudopilus component of the T2SS has ever been observed outside the cell under physiological conditions[48–50]. It is therefore likely that the tip of the pseudopilus never passes the periplasmic gate of the secretin and is used as a piston to push exoproteins into the periplasmic chamber of the secretin channel, possibly also to induce a conformational change in the secretin by interactions with the N3 constriction. Upon opening of the periplasmic gate, the pseudopilus may move the exoprotein through the opened gate and at the same time remain extended, serving as a plug to prevent channel leakage. Once the exoprotein is loaded into the extracellular chamber, the extracellular gate would open and the exoprotein can be released. After the exoprotein is released, the extracellular and periplasmic gates are likely to close, and the pseudopilus would no longer be required as a plug.

Our structures support a piston-driven secretion mechanism, with a crucial role for the constriction site in the periplasmic vestibule of GspD. This model is in line with current structural and biochemical studies. However, we must note that, although secretin interaction with the exoprotein has been reported before[14] and is also shown here, it is still not known (i) whether the pilus directly interacts with exoproteins with the aid of additional T2SS proteins or (yet-to-be-identified) adapters, and (ii) whether other T2SS proteins, such as GspC[51,52], also have a key role in inducing conformational changes of the secretin. Future studies must be carried out to answer these questions regarding the intriguing T2SS.

METHODS

Methods and any associated references are available in the online version of the paper at http://www.nature.com/nsmb/.

Accession codes. EM Database: The density map of *Vc*GspD has been deposited with accession number EMD-1763.

Note: Supplementary information is available on the Nature Structural & Molecular Biology website.

ACKNOWLEDGMENTS

We thank the Murdock Charitable Trust and the Washington Research Foundation for generous support of our cryo-EM facility. We are grateful to J. Sun, M. Gonen, B. Vollmar and S. Turley for contributions to the earlier stages of this work; M. Bagdasarian (Michigan State University) for a *Vc*GspD-containing plasmid; and J. DelaRosa for assistance with protein preparation. We thank A. J. Merz for helpful discussions. We thank N. Korotkova and P. Wallace for discussion of SPR experiments. Part of this work was conducted at the University of Washington NanoTech User Facility, a member of the US National Science Foundation (NSF) National Nanotechnology Infrastructure Network (NNIN). This research is supported by the US National Institutes of Health grant AI34501. The Gonen laboratory is supported in part by the Howard Hughes Medical Institute Early Career Scientist program.

AUTHOR CONTRIBUTIONS

T.G. and W.G.J.H. designed the research; K.V.K. cloned, expressed and purified protein samples, constructed the molecular models of the periplasmic rings of *Vc*GspD and of the pseudopilus and performed SPR experiments; S.L.R. collected and processed the cryo-EM data and prepared all figures; all authors wrote the manuscript.

COMPETING FINANCIAL INTERESTS

The authors declare no competing financial interests.

Published online at http://www.nature.com/nsmb/.
Reprints and permissions information is available online at http://npg.nature.com/reprintsandpermissions/.

1. Cianciotto, N.P. Type II secretion: a protein secretion system for all seasons. *Trends Microbiol.* **13**, 581–588 (2005).
2. Hirst, T.R., Sanchez, J., Kaper, J.B., Hardy, S.J. & Holmgren, J. Mechanism of toxin secretion by *Vibrio cholerae* investigated in strains harboring plasmids that encode heat-labile enterotoxins of *Escherichia coli*. *Proc. Natl. Acad. Sci. USA* **81**, 7752–7756 (1984).
3. Streatfield, S.J. *et al.* Intermolecular interactions between the A and B subunits of heat-labile enterotoxin from *Escherichia coli* promote holotoxin assembly and stability *in vivo*. *Proc. Natl. Acad. Sci. USA* **89**, 12140–12144 (1992).
4. Sixma, T.K. *et al.* Crystal structure of a cholera toxin-related heat-labile enterotoxin from *E. coli*. *Nature* **351**, 371–377 (1991).
5. Tauschek, M., Gorrell, R.J., Strugnell, R.A. & Robins-Browne, R.M. Identification of a protein secretory pathway for the secretion of heat-labile enterotoxin by an enterotoxigenic strain of *Escherichia coli*. *Proc. Natl. Acad. Sci. USA* **99**, 7066–7071 (2002).
6. Hirst, T.R. & Holmgren, J. Conformation of protein secreted across bacterial outer membranes: a study of enterotoxin translocation from *Vibrio cholerae*. *Proc. Natl. Acad. Sci. USA* **84**, 7418–7422 (1987).
7. Leece, R. & Hirst, T.R. Expression of the B subunit of *Escherichia coli* heat-labile enterotoxin in a marine *Vibrio* and in a mutant that is pleiotropically defective in the secretion of extracellular proteins. *J. Gen. Microbiol.* **138**, 719–724 (1992).
8. Chapon, V., Simpson, H.D., Morelli, X., Brun, E. & Barras, F. Alteration of a single tryptophan residue of the cellulose-binding domain blocks secretion of the *Erwinia chrysanthemi* Cel5 cellulase (ex-EGZ) via the type II system. *J. Mol. Biol.* **303**, 117–123 (2000).
9. Francetić, O. & Pugsley, A.P. Towards the identification of type II secretion signals in a nonacylated variant of pullulanase from *Klebsiella oxytoca*. *J. Bacteriol.* **187**, 7045–7055 (2005).
10. Voulhoux, R., Taupiac, M.P., Czjzek, M., Beaumelle, B. & Filloux, A. Influence of deletions within domain II of exotoxin A on its extracellular secretion from *Pseudomonas aeruginosa*. *J. Bacteriol.* **182**, 4051–4058 (2000).
11. Braun, P., Tommassen, J. & Filloux, A. Role of the propeptide in folding and secretion of elastase of *Pseudomonas aeruginosa*. *Mol. Microbiol.* **19**, 297–306 (1996).
12. Johnson, T.L., Abendroth, J., Hol, W.G. & Sandkvist, M. Type II secretion: from structure to function. *FEMS Microbiol. Lett.* **255**, 175–186 (2006).
13. Michel, G.P.F. & Voulhoux, R. The type II secretory system (T2SS) in Gram-negative bacteria: a molecular nanomachine for secretion of Sec and Tat-dependent extracellular proteins. in *Bacterial Secreted Proteins: Secretory Mechanisms and Role in Pathogenesis* (ed. Wooldridge, K.) 67–92 (Caister Academic, Norfolk, UK, 2009).
14. Shevchik, V.E., Robert-Baudouy, J. & Condemine, G. Specific interaction between OutD, an *Erwinia chrysanthemi* outer membrane protein of the general secretory pathway, and secreted proteins. *EMBO J.* **16**, 3007–3016 (1997).
15. Filloux, A., Michel, G. & Bally, M. GSP-dependent protein secretion in Gram-negative bacteria: the Xcp system of *Pseudomonas aeruginosa*. *FEMS Microbiol. Rev.* **22**, 177–198 (1998).
16. Sandkvist, M. Biology of type II secretion. *Mol. Microbiol.* **40**, 271–283 (2001).
17. Martin, P.R., Hobbs, M., Free, P.D., Jeske, Y. & Mattick, J.S. Characterization of *pilQ*, a new gene required for the biogenesis of type 4 fimbriae in *Pseudomonas aeruginosa*. *Mol. Microbiol.* **9**, 857–868 (1993).
18. Genin, S. & Boucher, C.A. A superfamily of proteins involved in different secretion pathways in Gram-negative bacteria: modular structure and specificity of the N-terminal domain. *Mol. Gen. Genet.* **243**, 112–118 (1994).
19. Brok, R. *et al.* The C-terminal domain of the *Pseudomonas* secretin XcpQ forms oligomeric rings with pore activity. *J. Mol. Biol.* **294**, 1169–1179 (1999).
20. Collins, R.F., Davidsen, L., Derrick, J.P., Ford, R.C. & Tonjum, T. Analysis of the PilQ secretin from *Neisseria meningitidis* by transmission electron microscopy reveals a dodecameric quaternary structure. *J. Bacteriol.* **183**, 3825–3832 (2001).

21. Opalka, N. *et al.* Structure of the filamentous phage pIV multimer by cryo-electron microscopy. *J. Mol. Biol.* **325**, 461–470 (2003).
22. Burghout, P. *et al.* Structure and electrophysiological properties of the YscC secretin from the type III secretion system of *Yersinia enterocolitica*. *J. Bacteriol.* **186**, 4645–4654 (2004).
23. Chami, M. *et al.* Structural insights into the secretin PulD and its trypsin-resistant core. *J. Biol. Chem.* **280**, 37732–37741 (2005).
24. Hodgkinson, J.L. *et al.* Three-dimensional reconstruction of the *Shigella* T3SS transmembrane regions reveals 12-fold symmetry and novel features throughout. *Nat. Struct. Mol. Biol.* **16**, 477–485 (2009).
25. Marlovits, T.C. *et al.* Assembly of the inner rod determines needle length in the type III secretion injectisome. *Nature* **441**, 637–640 (2006).
26. Marlovits, T.C. *et al.* Structural insights into the assembly of the type III secretion needle complex. *Science* **306**, 1040–1042 (2004).
27. Smith, J.M. Ximdisp—A visualization tool to aid structure determination from electron microscope images. *J. Struct. Biol.* **125**, 223–228 (1999).
28. Frank, J. *et al.* SPIDER and WEB: processing and visualization of images in 3D electron microscopy and related fields. *J. Struct. Biol.* **116**, 190–199 (1996).
29. Kocsis, E., Cerritelli, M.E., Trus, B.L., Cheng, N. & Steven, A.C. Improved methods for determination of rotational symmetries in macromolecules. *Ultramicroscopy* **60**, 219–228 (1995).
30. Grigorieff, N. FREALIGN: high-resolution refinement of single particle structures. *J. Struct. Biol.* **157**, 117–125 (2007).
31. Korotkov, K.V., Pardon, E., Steyaert, J. & Hol, W.G. Crystal structure of the N-terminal domain of the secretin GspD from ETEC determined with the assistance of a nanobody. *Structure* **17**, 255–265 (2009).
32. Finn, R.D. *et al.* Pfam: clans, web tools and services. *Nucleic Acids Res.* **34**, D247–D251 (2006).
33. Spreter, T. *et al.* A conserved structural motif mediates formation of the periplasmic rings in the type III secretion system. *Nat. Struct. Mol. Biol.* **16**, 468–476 (2009).
34. Chandran, V. *et al.* Structure of the outer membrane complex of a type IV secretion system. *Nature* **462**, 1011–1015 (2009).
35. Fronzes, R. *et al.* Structure of a type IV secretion system core complex. *Science* **323**, 266–268 (2009).
36. Christie, P.J. & Vogel, J.P. Bacterial type IV secretion: conjugation systems adapted to deliver effector molecules to host cells. *Trends Microbiol.* **8**, 354–360 (2000).
37. Vincent, C.D. *et al.* Identification of the core transmembrane complex of the *Legionella* Dot/Icm type IV secretion system. *Mol. Microbiol.* **62**, 1278–1291 (2006).
38. Ensminger, A.W. & Isberg, R.R. *Legionella pneumophila* Dot/Icm translocated substrates: a sum of parts. *Curr. Opin. Microbiol.* **12**, 67–73 (2009).
39. Schneidman-Duhovny, D., Inbar, Y., Nussinov, R. & Wolfson, H.J. PatchDock and SymmDock: servers for rigid and symmetric docking. *Nucleic Acids Res.* **33**, W363–W367 (2005).
40. Korotkov, K.V. & Hol, W.G. Structure of the GspK–GspI–GspJ complex from the enterotoxigenic *Escherichia coli* type 2 secretion system. *Nat. Struct. Mol. Biol.* **15**, 462–468 (2008).
41. Spagnuolo, J. *et al.* Identification of the gate regions in the primary structure of the secretin pIV. *Mol. Microbiol.* **76**, 133–150 (2010).
42. O'Neal, C.J., Amaya, E.I., Jobling, M.G., Holmes, R.K. & Hol, W.G. Crystal structures of an intrinsically active cholera toxin mutant yield insight into the toxin activation mechanism. *Biochemistry* **43**, 3772–3782 (2004).
43. Creze, C. *et al.* The crystal structure of pectate lyase peli from soft rot pathogen *Erwinia chrysanthemi* in complex with its substrate. *J. Biol. Chem.* **283**, 18260–18268 (2008).
44. Köhler, R. *et al.* Structure and assembly of the pseudopilin PulG. *Mol. Microbiol.* **54**, 647–664 (2004).
45. Yanez, M.E., Korotkov, K.V., Abendroth, J. & Hol, W.G. Structure of the minor pseudopilin EpsH from the type 2 Secretion system of *Vibrio cholerae*. *J. Mol. Biol.* **377**, 91–103 (2008).
46. Yanez, M.E., Korotkov, K.V., Abendroth, J. & Hol, W.G. The crystal structure of a binary complex of two pseudopilins: EpsI and EpsJ from the type 2 secretion system of *Vibrio vulnificus*. *J. Mol. Biol.* **375**, 471–486 (2008).
47. Korotkov, K.V. *et al.* Calcium is essential for the major pseudopilin in the type 2 secretion system. *J. Biol. Chem.* **284**, 25466–25470 (2009).
48. Durand, E. *et al.* Type II protein secretion in *Pseudomonas aeruginosa*: the pseudopilus is a multifibrillar and adhesive structure. *J. Bacteriol.* **185**, 2749–2758 (2003).
49. Durand, E. *et al.* XcpX controls biogenesis of the *Pseudomonas aeruginosa* XcpT-containing pseudopilus. *J. Biol. Chem.* **280**, 31378–31389 (2005).
50. Vignon, G. *et al.* Type IV-like pili formed by the type II secreton: specificity, composition, bundling, polar localization, and surface presentation of peptides. *J. Bacteriol.* **185**, 3416–3428 (2003).
51. Bouley, J., Condemine, G. & Shevchik, V.E. The PDZ domain of OutC and the N-terminal region of OutD determine the secretion specificity of the type II out pathway of *Erwinia chrysanthemi*. *J. Mol. Biol.* **308**, 205–219 (2001).
52. Korotkov, K.V., Krumm, B.E., Bagdasarian, M. & Hol, W.G. Structural and functional studies of EpsC, a crucial component of the type 2 secretion system from *Vibrio cholerae*. *J. Mol. Biol.* **363**, 311–321 (2006).

ONLINE METHODS

Expression and purification of recombinant *Vc*GspD channels. The full-length gene of *V. cholerae* GspD (*Vc*GspD) was cloned into the pET-22b(+) vector from pMMB710 plasmid (a gift from M. Bagdasarian) to encode a C-terminal hexahistidine tag. *Vc*GspD was expressed in the Tuner(DE3)pLacI strain by growing the cells to an absorbance at 600 nm (A_{600}) of 0.8 and induced with 0.1 mM IPTG. Cells were harvested 3 h after induction, resuspended in 20 mM Tris-HCl (pH 7.8) and 300 mM NaCl and disrupted using a French press. The membrane fraction was isolated by ultracentrifugation, and membrane proteins were solubilized using *N*-dodecyl-*N*,*N*′-dimethylammonio-1-propanesulfonate (SB3-12). *Vc*GspD was purified using nickel-affinity and size-exclusion chromatography (**Fig. 1a,b**). The N-terminal sequencing results (not shown) indicated that the signal peptide was intact. This has also been observed upon replacement of the native signal *Vc*GspD sequence with *pelB* signal sequence. Those results suggest that *Vc*GspD is targeted to the inner membrane in our expression system, similar to *Ko*GspD in the absence of a cognate pilotin protein GspS[53]. It should be noted that no pilotin homologs have been identified so far in the *V. cholerae* genome.

Electron cryomicroscopy and image processing. ***Vc*GspD** was prepared for cryo-EM by applying a 2-µl drop of sample (~0.05 mg ml^{-1}) to a negatively charged Quantifoil holey carbon specimen grid (Quantifoil) overlaid with a continuous layer of carbon. The sample was blotted with filter paper and plunged into liquid ethane using a Vitrobot (FEI). The frozen specimen was loaded into a Gatan cryo holder and inserted into an FEI Tecnai F20 microscope, equipped with a field-emission gun operated at 200 kV under low-dose conditions. Images were recorded on film (Kodak SO-163) at a magnification of 50,000× and at defocus values ranging from 1.5 µm to 5.0 µm. The film was digitized with a 6.9-µm step size and binned twice, yielding a final pixel size of 2.54 Å per pixel. Thon rings in the power spectra were used to select only those micrographs that were free of drift or significant astigmatism. The contrast transfer function (CTF) parameters were determined for each micrograph using the program CTFTILT[54]. Approximately 20,000 particles were selected using Ximdisp[27] and processed in SPIDER[28] for generating multivariate reference-free class averages. Rotational symmetry of *Vc*GspD was determined from axially oriented particles, using real-space symmetry averaging in EMAN[55] and rotational power spectra analysis using RotaStat[29] (**Supplementary Fig. 1**).

Three-dimensional reconstruction and refinement of *Vc*GspD. A low-resolution density map of *Vc*GspD was initially obtained from negatively stained particles in SPIDER[28] and used as an initial search model for our best 10,000 particle images in FREALIGN v.7[30]. Search and refine protocols were used in FREALIGN to determine initial Euler angles and *x*, *y* shifts relative to the initial search model for each particle and then refined with an applied C12 rotational symmetry through consecutive rounds of parameter refinement and three-dimensional reconstruction until no improvement in alignment parameters was observed. The nominal resolution of the final reconstruction was estimated from where the FSC curve fell to a value of 0.5 (ref. 56), corresponding to 19 Å (**Supplementary Fig. 2**). The final map was filtered to 19 Å and normalized using MAPMAN[57]. The map was visualized and prepared for figures using UCSF Chimera[58] at a contour level of 3.4σ, corresponding to an approximate 0.9-MDa volume[59]. **Figure 2c** was prepared using a 2.4σ contour level to show the spoke features observed in projection averages. Our C12 symmetry assignment of *Vc*GspD was supported by comparison with the results obtained when alternative symmetries were applied to the reconstruction (**Supplementary Fig. 1**).

Creation of periplasmic *Vc*GspD rings, cholera toxin and pseudopilus models. The modeling of C12-symmetry periplasmic *Vc*GspD rings was performed using the program SymmDock[39], using methods previously described[47]. A model of the pseudopilus was used based on the helical parameters from the GspK–GspI–GspJ complex, by adding additional pseudopilins to the tip[40]. A molecular model for the export of a secreted protein by the T2SS was then obtained by aligning the helical axis of the pseudopilus with the 12-fold symmetry axis of the GspD reconstruction and placing the structure of cholera toxin[42] on top of the GspK–GspI–GspJ tip, with the fivefold axis of symmetry coinciding with the 12-fold and helical axes (**Fig. 5**).

Fitting of models into the *Vc*GspD reconstruction. Periplasmic *Vc*GspD ring models were fit into the density map of *Vc*GspD as follows. The ten lowest-energy ring models for each of the N0/1, N2 and N3 domains calculated by SymmDock were initially placed into the density map of *Vc*GspD (**Supplementary Fig. 7**). The N0/N1 domain was treated as a single complex, and the ring model for this domain was placed at the very bottom of the periplasmic domain of the *Vc*GspD map, with the N terminus pointed downward (toward the periplasm). The N2 and N3 ring models were treated separately because these are tethered by flexible linkers, and they were placed in an N- to C-terminal (head-to-tail) fashion. These initial placements were optimized by automated fitting procedures in UCSF Chimera[58]. The ring models for each domain with the best correlation to the experimental map were selected. The final N0–N3 periplasmic domain model gave a cross-correlation score of 0.65 compared to the experimental map (**Supplementary Fig. 7**).

Surface plasmon resonance studies. The B-pentamer of the heat-labile enterotoxin (LTB_5), the *Ec*GspD fragment 1–237 (peri-GspD) corresponding to the N0-N1-N2 subdomains and the trimeric pseudopilus tip complex *Ec*GspK–GspI–GspJ were each expressed and purified as described[31,40,60]. peri-GspD was immobilized on a CM5 research-grade sensor chip (GE Healthcare) by amine-coupling chemistry using the manufacturer's protocols, and LTB_5 and *Ec*GspK–GspI–GspJ were used as the analyte. SPR measurements were carried out in HBS-EP buffer (10 mM HEPES (pH 7.4), 150 mM NaCl, 3 mM EDTA, 0.005% P-20 surfactant) at 25 °C using the Biacore T100 system (GE Healthcare). The interaction of LTB_5 with peri-GspD was confirmed using immobilized LTB_5 and peri-GspD as analyte; however, in this case no steady-state binding was observed owing to homophilic GspD interactions (data not shown). Data were analyzed with the Biacore T100 Evaluation software, v. 2.0.1.

Software used for figure preparation. All figures were prepared for publication using Photoshop, v. 9.0.2.

53. Guilvout, I., Chami, M., Engel, A., Pugsley, A.P. & Bayan, N. Bacterial outer membrane secretin PulD assembles and inserts into the inner membrane in the absence of its pilotin. *EMBO J.* **25**, 5241–5249 (2006).
54. Mindell, J.A. & Grigorieff, N. Accurate determination of local defocus and specimen tilt in electron microscopy. *J. Struct. Biol.* **142**, 334–347 (2003).
55. Ludtke, S.J., Baldwin, P.R. & Chiu, W. EMAN: semiautomated software for high-resolution single-particle reconstructions. *J. Struct. Biol.* **128**, 82–97 (1999).
56. Stewart, P.L., Chiu, C.Y., Haley, D.A., Kong, L.B. & Schlessman, J.L. Review: resolution issues in single-particle reconstruction. *J. Struct. Biol.* **128**, 58–64 (1999).
57. Kleywegt, G.J. & Jones, T.A. xdlMAPMAN and xdlDATAMAN—programs for reformatting, analysis and manipulation of biomacromolecular electron-density maps and reflection data sets. *Acta Crystallogr. D Biol. Crystallogr.* **52**, 826–828 (1996).
58. Pettersen, E.F. *et al.* UCSF Chimera—a visualization system for exploratory research and analysis. *J. Comput. Chem.* **25**, 1605–1612 (2004).
59. Matthews, B.W. Solvent content of protein crystals. *J. Mol. Biol.* **33**, 491–497 (1968).
60. Mitchell, D.D., Pickens, J.C., Korotkov, K., Fan, E. & Hol, W.G. 3,5-Substituted phenyl galactosides as leads in designing effective cholera toxin antagonists; synthesis and crystallographic studies. *Bioorg. Med. Chem.* **12**, 907–920 (2004).

doi:10.1038/nsmb.1910